Distribution of biomass dynamics in relation to tree size in forests across the world - Supporting Information

Camille Piponiot Kristina J. Anderson-Teixeira Stuart J. Davies David Allen
Norman A. Bourg David F.R.P. Burslem Dairon Cárdenas
Chia-Hao Chang-Yang George Chuyong Susan Cordell

Handanakere Shivaramaiah Dattaraja Álvaro Duque Sisira Ediriweera
Corneille Ewango Zacky Ezedin Jonah Filip Christian Giardina
Robert Howe Chang-Fu Hsieh Stephen Hubbell Faith M. Inman-Narahari
Akira Itoh David Jánik David Kenfack Kamil Král James A. Lutz
Jean-Remy Makana Sean M. McMahon William McShea Xiangcheng Mi
Mohizah Bt. Mohamad Vojtech Novotný Michael J. O'Brien
Rebecca Ostertag Geoffrey Parker Rolando Pérez Haibao Ren
Glen Reynolds Mohamad Danial Md Sabri Lawren Sack Ankur Shringi
Sheng-Hsin Su Raman Sukumar I-Fang Sun Hebbalalu S. Suresh
Duncan W. Thomas Jill Thompson Maria Uriarte John Vandermeer
Yunquan Wang Ian M. Ware George D. Weiblen Timothy J. S. Whitfeld
Amy Wolf Tze Leong Yao Mingjian Yu Zuoqiang Yuan Jess Zimmerman
Daniel Zuleta Helene C. Muller-Landau

Article acceptance date 5 October 2021

Contents

Dataset S1

Total aboveground woody biomass (AGB; Mg ha^{-1}), aboveground woody productivity (AWP; Mg ha^{-1} yr^{-1}), and aboveground woody mortality (AWM; Mg ha^{-1} yr^{-1}) for each site and site-specific diameter classes (in cm), as presented in the figures. These size classes have been chosen to improve visualization (see definition of diameter classes in Appendix C). We provide the value over the entire plot (column: total)

and the lower and upper bounds of the 95% confidence interval (columns: lower_bound and upper_bound), estimated after bootstrapping 20 x 20 m quadrats with 1000 replicates. Biomass units here are for oven-dry biomass as estimated from allometric equations (see the main text Materials and Methods section). Dataset S1 is provided as a separate file.

Dataset S2

Total aboveground woody biomass (AGB; Mg ha^{-1}), aboveground woody productivity (AWP; Mg ha^{-1} yr^{-1}), and aboveground woody mortality (AWM; Mg ha^{-1} yr^{-1}) for each site by standardized diameter classes of $[1, 5)$, $[5, 10)$, $[10, 20)$, $[20, 30)$, $[30, 40)$, $[40, 50)$, $[50, 100)$, $[100, 200)$, and $[200, +\infty)$ cm DBH. We provide the value over the entire plot (column: total) and the lower and upper bounds of the 95% confidence interval (columns: lower_bound and upper_bound), estimated after bootstrapping 20 x 20 m quadrats with 1000 replicates. Biomass units here are for oven-dry biomass as estimated from allometric equations (see the main text Materials and Methods section). Dataset S2 is provided as a separate file.

Dataset S3

Median, dispersion and skewness of AGB, AWP and AWM distributions at each site. The median is the diameter (in cm) at which 50% of the total stock or flux is below, and 50% above. We calculated the dispersion as the quartile coefficient of dispersion (dimensionless), i.e. the difference between the third and first quartiles, divided by the sum of the first and third quartiles. We calculated the skewness as Pearson's first skewness coefficient (dimensionless), i.e. the difference between the mean and median of the distribution, divided by its standard deviation. These summary statistics (median, dispersion and skewness) were calculated based on 1-cm wide diameter classes. Dataset S3 is provided as a separate file.

Appendix A - Site-specific information on ForetGEO sites used in this study

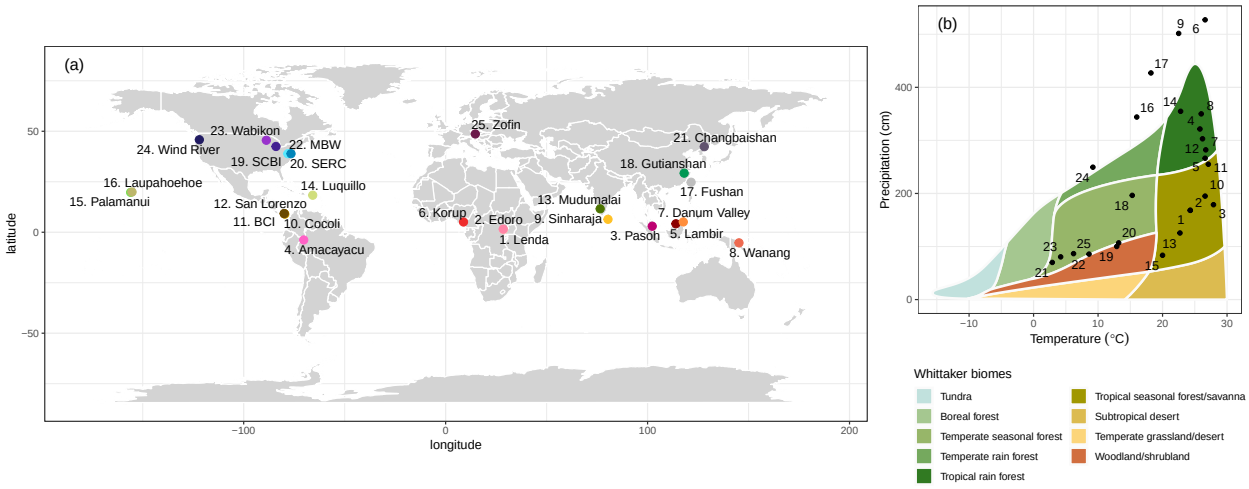

Figure S1: Location and environmental conditions of study sites. (a) Map of site locations, with site number and color (from red to blue) increasing with increasing absolute latitude. (b) Site distribution on a Whittaker biome diagram of mean annual precipitation and mean annual temperature (Whittaker, 1975); sites are numbered as on the map.

Table S1: Plot initiation papers

Site	Citation
Barro Colorado Island	Hubbell *et al.* (1999)
Changbaishan	Yuan *et al.* (2016)
Cocoli	Condit *et al.* (2004)
Fushan	Su *et al.* (2010)
Gutianshan	Chen *et al.* (2010)
Ituri (Edoro and Lenda)	Makana & C. Thomas (2004)
Korup	Kenfack *et al.* (2007)
Lambir	Lee *et al.* (2002)
Laupahoehoe and Palamanui	Inman-Narahari *et al.* (2010)
Luquillo	Zimmerman *et al.* (2010)
Michigan Big Woods	Allen *et al.* (2019)
Mudumalai	Sukumar *et al.* (2004)
Pasoh	Manokaran & LaFrankie (1990)
San Lorenzo	Condit *et al.* (2004)
SCBI	Bourg *et al.* (2013)
SERC	Mcmahon & Parker (2015)
Wabikon	Wang *et al.* (2011)
Wanang	Vincent *et al.* (2015)
Wind River	Lutz *et al.* (2013)
Zofin	Janík *et al.* (2016)

Table S2: Disturbances at the ForestGEO sites used in this study. Information was provided by the principal investigators at the sites.

Site	Disturbance history	Current natural disturbances	Current anthropogenic disturbances
Amacayacu	No evidence of major historical disturbance; 14C dating of charcoal and phytolith analysis obtained from soil cores in Amacayacu indicated that this forest has not had fire disturbance in the last 1630 years (Heijink *et al.*, 2020).	Droughts (Zuleta *et al.*, 2017); windstorms; infrequent flooding: the swampy area ($\simeq$ 7ha) is seasonally flooded due to the interaction of poor drainage of soils in the bottom part of internal valleys, the drainage of streamlets during the wet season, and the high seasonal level of the Amazon River's water table (Zuleta *et al.*, 2020).	The plot is within a National Natural Park and there is no evidence of anthropogenic disturbance.
Barro Colorado Island	The 50-ha Plot has been continuously forested for at least 1000 years; in pre-Columbian times, there were two small camps (both over 600 years old) on the site of the 50-ha plot, but there is no evidence of agriculture or forest clearing. Our analyses excluded 2 ha of young forest on the northern edge of the 50-ha plot (Harms *et al.*, 2001) that were cleared during the 19th century and estimated to be no more than 30 years old by Enders (1935).	Infrequent local windstorms sometimes fell a hectare or more of forest (return time: 1000-5000 yrs); El Nino-related droughts (return time 10-20 yrs) increase stem mortality to around 4%, most recent droughts: 1983 and 1998.	Disconnected from contiguous forest upon creation of Panama Canal (habitat fragmentation).
Changbaishan	Previously logged forest; logging stopped around 1830.		Non-wood forest product collection.
Cocoli	Secondary forest of about 100 years (Condit, 1998).	El Nino-related droughts, last drought (1998) increased stem mortality to 6.44% during that year.	
Danum Valley	No evidence of major historical disturbance, although there is archaeological evidence of pre-historic human occupation in the surrounding area.	A small part of the plot has a low canopy cover and reduced tree density which might be indicative of edaphic constraints or waterlogging; occasional severe El Nino driven droughts (Nunes *et al.*, 2019).	There is limited direct human pressure in the area.

Site	Disturbance history	Current natural disturbances	Current anthropogenic disturbances
Edoro	Widespread presence of charcoal in the soil indicates fire disturbance in the past.	Windstorms; elephants.	Some very limited hunting pressure.
Fushan	No evidence of major historical disturbance. The plot is remote and located near a well-protected area, the Hapen Nature Reserve, which was established in 1986.	Frequent typhoons - averages 0.49 major typhoons ($\geq$ category 3 on the Saffir–Simpson scale) annually (Lin *et al.*, 2011).	No evidence of anthropogenic disturbance.
Gutianshan	No evidence of major historical disturbance.	Occasional ice storms and fires.	
Korup	No evidence of major historical disturbance.		Hunting pressure moderate to severe.
Lambir	No evidence of major historical disturbance. Forest heavily impacted by hunting during the 1990s and early 2000s causing the extinction of some primate seed dispersers (gibbons), but more recent camera trapping has found high occupancy of muntjac, mouse deer, and short-tailed macaque, medium occupancy of other species (e.g. bearded pig). Landslide in 1963.	El Nino droughts affect seedling regeneration and tree mortality.	The plot is within the Lambir Hills National Park and there is no evidence of anthropogenic disturbances.
Laupahoehoe	Following contact around 1700, native Hawaiian koa trees may have been occasionally harvested but there is no documented history of an actual harvest in the plot itself. After the non-native trees were mapped in 2009, they were girdled and sprayed with herbicide.	Droughts; windstorms.	Hunting of feral ungulates. Accidental introduction of invasive plant species.
Lenda	Widespread presence of charcoal in the soil indicates fire disturbance in the past.	Windstorms; elephants.	Some very limited hunting pressure.

Site	Disturbance history	Current natural disturbances	Current anthropogenic disturbances
Luquillo	The plot has been covered by forest since the 1930s; before then, 1.16 ha of the 16-ha plot was clearcut and later trees were planted to recover the canopy. 9.6 ha was variably cut over and planted in places with coffee and fruit trees. Since 1934 the forest has been allowed to grow naturally. 5.24 ha has always been in forest but some of this area had minimal selective logging in the 1940's. In the 1960's a small gap was created (320 m^2) as part of an experiment.	Severe hurricanes - return time: 50-60 years; very severe hurricanes in 1928 and 1932 then also 1989 (Hugo), 1998 (Georges) and 2017 (Maria); landslides affect, on average, less than 1% of the plot forest area at any time and landslides are mainly related to heavy rainfall events and hurricanes.	Black rat and mongoose were introduced to the forest in the past, and this represents an indirect form of human disturbance. No current human disturbance except from plot census activities.
Michigan Big Woods	Presumed regular burning by Native Americans, prior to fire suppression by White settlers. After that it was a pastured woodlot until around 100 years ago. Large oak cohort is about 150 years old and being replaced by more mesophytic species.	Periodic gypsy moth defoliation events, with small effects on understory growth.	Invasive shrubs abundant in parts of the understory.
Mudumalai	A long history of selective timber extraction ended in 1968; extraction of non-timber forest products ended around 1990; hunting pressure on large mammals was prevalent in the past but has been low or non-existent since about 2000.	Frequent understory fires - 1989, 1991, 1992, 1994, 1996, 2002 and 2010 in the 50 ha plot; elephant browsing.	Invasive species abundant in the understory.
Palamanui	After the non-native trees were mapped, they were girdled and sprayed with herbicide. No evidence of other historical disturbance.	Drought; windstorms.	Occasional ingress of feral ungulates; accidental introduction of invasive weeds; wildfire.
Pasoh	No evidence of major historical disturbance; gazetted as a forest reserve in 1917 and the core part in which the plot lies has remained undisturbed forest since then. The core part consists of 12 forest compartments totaling 1840 hectares and has been protected as a research forest by the Negeri Sembilan State Government since 1969.	Wind squalls can sometimes upend groups of trees	Surrounded by logging concessions and oil palm plantations; low intensity hunting and non-timber forest products extraction.

Site	Disturbance history	Current natural disturbances	Current anthropogenic disturbances
San Lorenzo	Forest established for 200 years or more, since the largest trees are of slow-growing species (*Manilkara bidentata*, *Brosimum utile*).	El-Nino related droughts: stem mortality after the 1998 drought was 4.88% yr^{-1}.	Signs of human impact in the area - the largest Manilkara in the plot has been slashed many times for latex, and the northern hectare of the plot was obviously cleared recently. The plot has been subject to some logging or clearing activity during the last 150 yr.
Sinharaja	The Reserve has been impacted by selective logging in the 1970's, but not in the plot. Locally-abundant canopy species experienced massive die-off between 1993 and 1998.	Occasional strong wind storms; small/medium size landslides (< 1ha) occasionally occur during the heavy south-west monsoon period (May-July).	Sinharaja is Man and Biosphere Reserve hence anthropogenic disturbances are very limited, however, extraction of non-timber forest products occurs on the margins of the forest.
Smithsonian Conservation Biology Institute	Land on which the plot is located was mostly private farmland in the 19th century. Some level of timber harvest occurred throughout this history. The plot was left relatively undisturbed since ownership was transferred to the Smithsonian in 1975. Dendrochronological data from 492 tree cores suggested the major canopy trees established around 1900, but scattered trees of several species existed as early as 1777. History is detailed in Bourg *et al.* (2013).		Exotic pests and pathogens have been the largest source of disturbance in recent decades. Small gravel road through the plot is maintained, as is a 4-ha deer exclosure (since 1990). Plot is within fenced property (since 1980).
Smithsonian Environmental Research Center	Secondary forest of about 130 years: former dairy farm - initiation of post-disturbance cohort (natural) around 1890. Surrounding forest of about 80 years.		
Wabikon	Logged extensively in early 1900's. Selective cutting through about 1985; designated as a state natural area in 2007.	Windstorm-induced treefall gaps.	Regulated hunting of white-tailed deer occurs annually; black bear and other large carnivores also are harvested regionally.

Site	Disturbance history	Current natural disturbances	Current anthropogenic disturbances
Wanang	No evidence of logging or shifting cultivation (subsistence agriculture).	Unstable terrain with frequent landslides create gaps ranging 0.05-1.0 ha.	Considerable hunting pressure.
Wind River	High severity fire around 1490.	Typical disturbance regime is high-severity, infrequent fire, with frequent windstom-induced treefall gaps (Lutz *et al.*, 2013).	The T. T. Munger Research Natural Area (RNA) was established in 1932, and the forest has been formally protected since that time. Ungulates and their predators are present and hunted nearby, but not in the RNA.
Zofin	Severe windstorm Kyrill touched the plot on 18 January 2007.	Typical disturbance regime is frequent small wind-induced treefall gaps, with infrequent high-severity windstorms. The mean disturbance rate was 11.0% canopy loss per decade (maximum 33.7%) in the core zone (Šamonil *et al.*, 2013). Recent effect of high game pressure (over-browsing).	No evidence of major anthropogenic disturbance - under strict protection since 1838. Bordering forests were directly affected by humans after 1800.

Appendix B - Methods for calculating biomass fluxes

Appendix B.1 – General methods

Methods S1

We corrected for the bias associated with census interval length (which varies within and among sites) by estimating instantaneous aboveground woody productivity and mortality for each size class and 20 x 20 m quadrat using equations 3 and 4 from Table 1 in Kohyama *et al.* (2019):

$$AWP = \frac{[1-(AGBs_0/AGB_T)^{1/T}](AGB_T - AGB_0)}{T[1-(AGB_0/AGB_T)^{1/T}]}$$

$$AWM = \frac{[1-(AGBs_0/AGB_0)^{1/T}](AGB_T - AGB_0)}{T[(AGB_T/AGB_0)^{1/T}-1]}$$

where T is the census interval (in years), per quadrat; AGB_0 is the initial (first census) biomass of all trees in the size class (in Mg ha^{-1}); AGB_T is the biomass of all trees in the size class at the 2nd census; $AGBs_0$ is the initial biomass of all survivors, i.e. trees that survived and stayed in the size class in both censuses.

In the case of stems that had a change in height of measurement between two censuses, or for which the change in DBH was $\leq$ -0.5 cm yr^{-1} or $\geq$ 5 cm yr^{-1}, their DBH change and corresponding AGB change were substituted with the respective expected value, calculated from DBH changes of all other stems in the same site and size class, as detailed below (Methods S2).

Appendix B.2 – Gap-filling DBH growth

Methods S2

To calculate the expected AGB change for a given site and size class, we first characterized the distribution of DBH changes for that size class. To remove the skewness of the distribution of DBH changes, we applied a transformation with the modulus function, as recommended by Condit *et al.* (2017), with a parameter $\lambda = 0.5$. The distribution of transformed DBH changes in each diameter class can then be approximated with a normal distribution. We calculated the expected change in AGB for any given stem by integrating the AGB allometry with the expected DBH change distribution for the appropriate site and size class, given that stem's initial DBH.

The modulus function used to transform DBH changes is defined as:

$$mod(x) = \begin{cases} x^{\lambda} & \text{if } x \geq 0 \\ -(-x)^{\lambda} & \text{if } x < 0 \end{cases} \quad (1)$$

The value of parameter λ was set to 0.5, for which the distribution of modulus-transformed DBH growth is well-approximated by a normal distribution (Figure S2 illustrates how the value of parameter λ was set for BCI, and Figure S3 illustrates the normality of the modulus-transformed DBH growth in other sites). Thus, we approximated the distribution of modulus-transformed DBH changes in site s and diameter class b with a normal distribution of mean $\mu_{s,b}$ and standard deviation $\sigma_{s,b}$.

The expected DBH in site s and diameter class b change is then:

$$[E(dDBH)]_{s,b} = \int_{-\infty}^{+\infty} mod^{-1}(x) \cdot \varphi\left(\frac{x-\mu_{s,b}}{\sigma_{s,b}}\right) \cdot dx \quad (2)$$

For each stem i in site s and diameter class b with initial DBH D_i, we calculated the expected AGB change as

$$[E(dAGB)]_i = \int_{dmin}^{+\infty} \left(AGB(D_i + mod^{-1}(x)) - AGB(D_i)\right) \cdot \frac{\varphi\left(\frac{x-\mu_{s,b}}{\sigma_{s,b}}\right)}{1-\Phi\left(\frac{x-\mu_{s,b}}{\sigma_{s,b}}\right)} \cdot dx \tag{3}$$

with $D_i + mod^{-1}(dmin) = 0 \Rightarrow dmin = -D_i^{\lambda}$ (to avoid negative AGB values), AGB is the allometric equation used in site s, and φ and Φ are respectively the probability and cumulative density functions of the standard normal distribution.

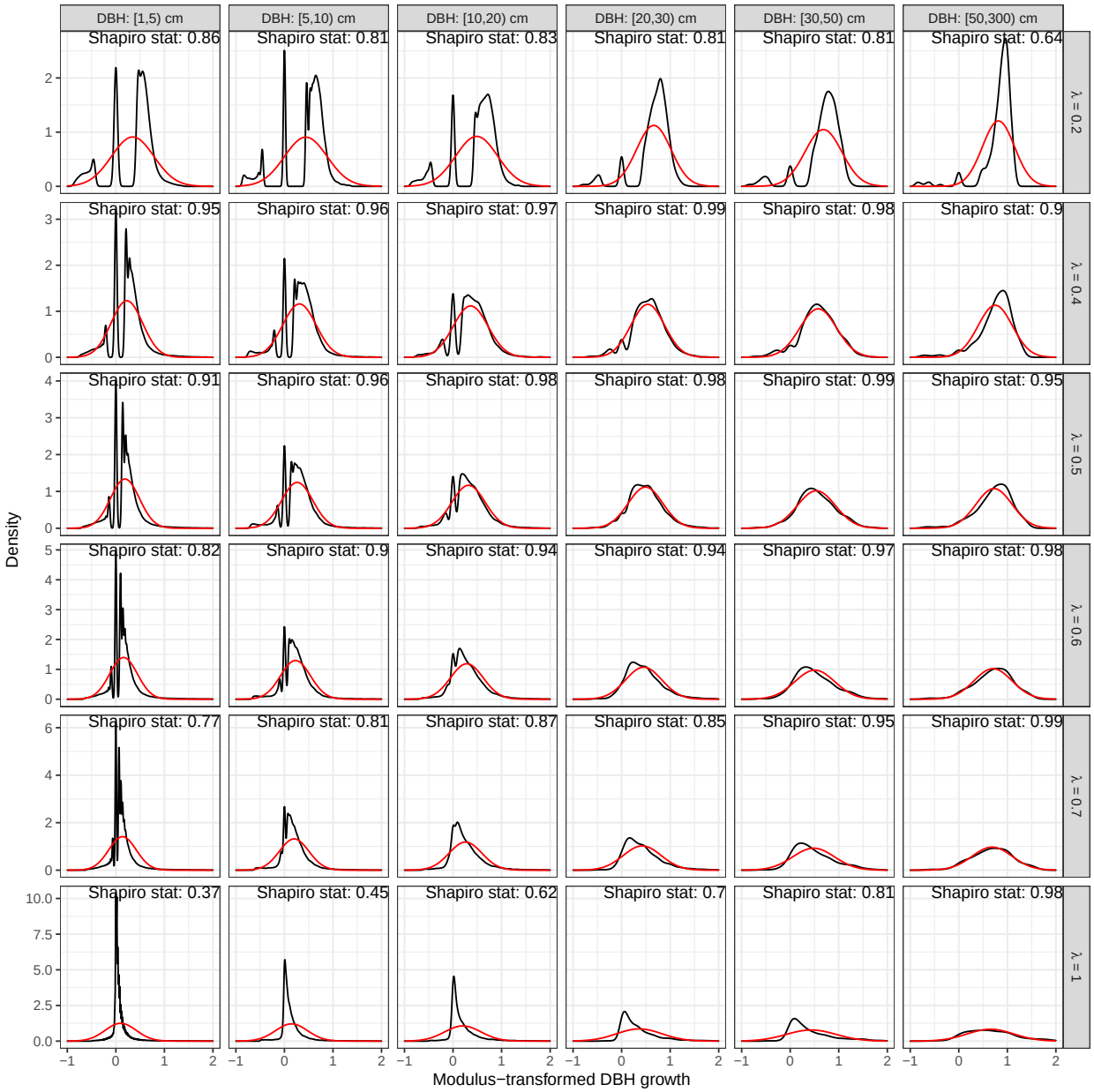

Figure S2: Distribution of modulus-transformed DBH growth values from individual trees in the BCI data as an example. Stems were divided into six size classes based on DBH (panels from left to right; the lower limit is included and the upper limit is excluded from the size class), and for each size class DBH growth was modulus-transformed using six values of parameter λ, ranging 0.2-1 (panels from top to bottom; note that when $\lambda = 1$, the modulus function is the identity function and the data is thus not transformed). The red line is the density of the normal distribution with same mean and standard deviation as the modulus-transformed data. The Shapiro-Wilk test statistic is provided as a measure of the normality of the data. For most size classes, the Shapiro-Wilk test statistic was highest when $\lambda = 0.5$, meaning that the distribution of the transformed data was closest to a normal distribution for this parameter value.

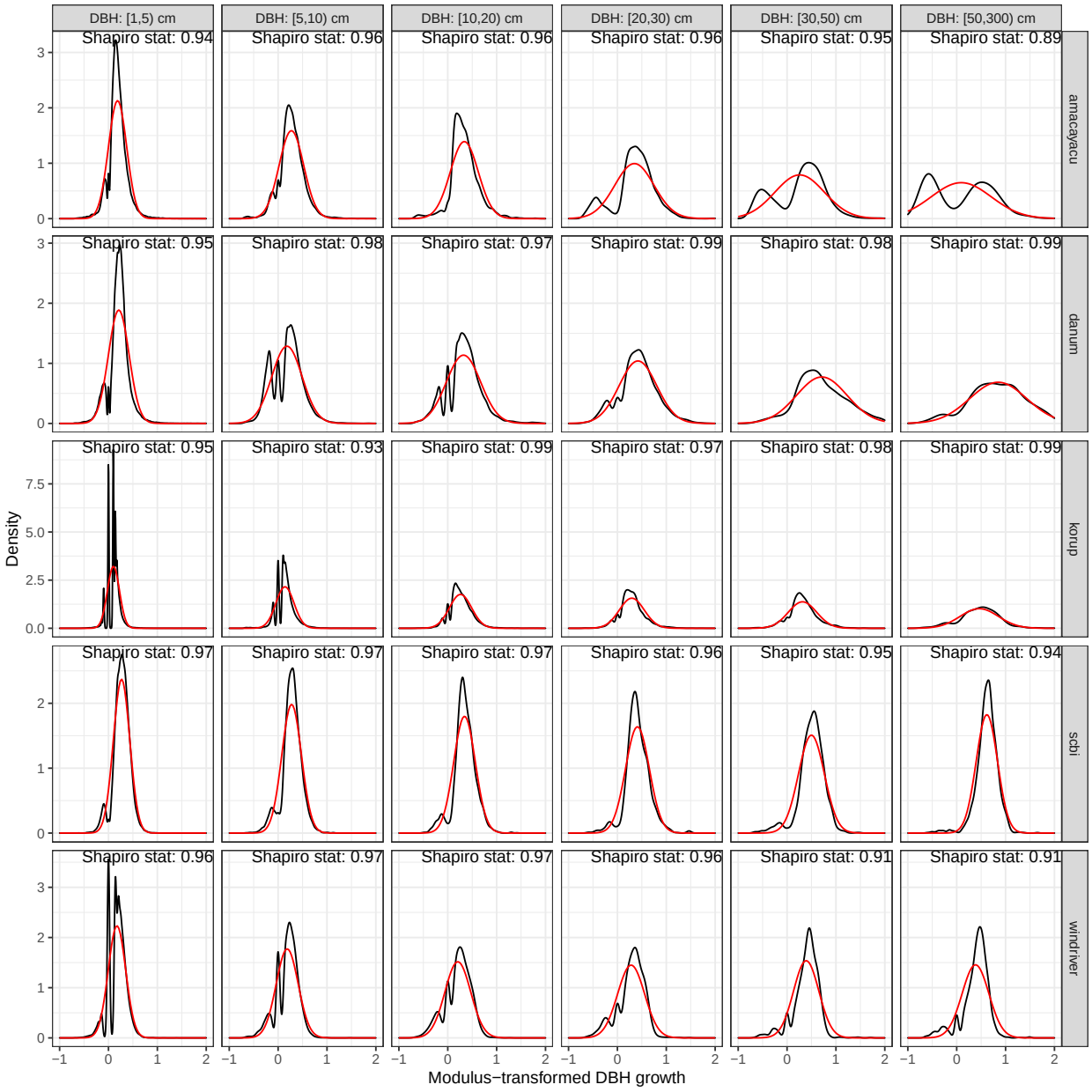

Figure S3: Distribution of modulus-transformed DBH growth values from individual trees in five different sites (panels from top to bottom), with parameter λ set to 0.5. Stems were divided into six size classes based on DBH (panels from left to right). The red line is the density of the normal distribution with same mean and standard deviation as the modulus-transformed data. The Shapiro-Wilk test statistic is provided as a measure of the normality of the data. The three tropical sites shown (Amacayacu, Danum Valley and Korup) are located in the three main tropical forest basins (Amazonia, South East Asia and Central Africa respectively), and the two temperate sites (SCBI and Wind River) are in different biomes: broadleaf-dominated deciduous temperate forests and conifer-dominated temperate rainforests, respectively.

Appendix C - Definition of diameter classes for graphing

Methods S3

The definition of diameter classes presented in graphs here is specific to our dataset, and its only purpose is to improve the visualization of the data by finding a suitable compromise between a number of diameter classes large enough to visualize useful information on size-related stand dynamics, and small enough to limit the influence of stochastic variability due to small sample sizes. Diameter classes were defined separately for each site in a 3-step process: first, the number of diameter classes per site is defined based on the total number of stems in the site, then the target proportions of the total number of stems in each diameter class are defined such that they decrease with increasing diameter, and finally the bounds of diameter classes are chosen to best achieve the target numbers of stems.

Step 1: The number of diameter classes, Nb_s, in site s is determined from the total number of stems in that site, $Ntot_s$, as

$$Nb_s = \lceil 30 \cdot \left(1 - exp(-Ntot_s \cdot 2 \cdot 10^{-5})\right) \rceil \tag{4}$$

where $\lceil\ \rceil$ is the ceiling function. The maximum number of diameter classes is thus 30 (sites with more than 86,000 stems have 30 diameter classes, and sites with fewer stems have fewer diameter classes). The numbers of diameter classes for each site are reported in Table S3.

Step 2: The target proportion of the total number of stems in the ith diameter class in site s, $P_{s,i}$, is then defined by:

$$P_{s,i} = F\left(\frac{i}{Nq_s}, \alpha = 1, \beta = 4\right),\ \forall i \in [1, Nq_s] \tag{5}$$

where $F(x, \alpha = 1, \beta = 4)$ is the distribution function (or cumulative density function) of the beta distribution, with shape parameters $\alpha = 1$ and $\beta = 4$. Parameter values were chosen empirically to have large-enough diameter classes for small diameters. which have more stems, and small-enough diameter classes for large diameters, which have fewer stems but contribute more to AGB stocks and fluxes (see Figure S4).

Step 3: Boundaries of each diameter class are chosen to achieve the target proportions as best as possible, considering the limits of precision of the empirical data, that is, many trees measured as being exactly the same diameter, especially for small diameters.

Diameter classes that had < 20 stems in the first census were merged with the next smaller diameter class.

Table S3: Total number of diameter classes per site, before and after merging when necessary (to avoid diameter classes with < 20 stems).

Site	N diameter classes before merging	N diameter classes after merging
Amacayacu	30	27
BCI	30	28
Changbaishan	28	25
Cocoli	11	9
Danum Valley	30	28
Fushan	30	27
Gutianshan	30	28
Korup	30	28
Lambir	30	29
Laupahoehoe	12	11
Luquillo	24	21
MBW	20	17
Mudumalai	16	15
Palamanui	22	19
Pasoh	30	28
SCBI	26	23
SERC	22	19
San Lorenzo	17	14
Sinharaja	30	27
Wabikon	27	24
Wanang	30	28
Wind River	22	19
Zofin	28	20

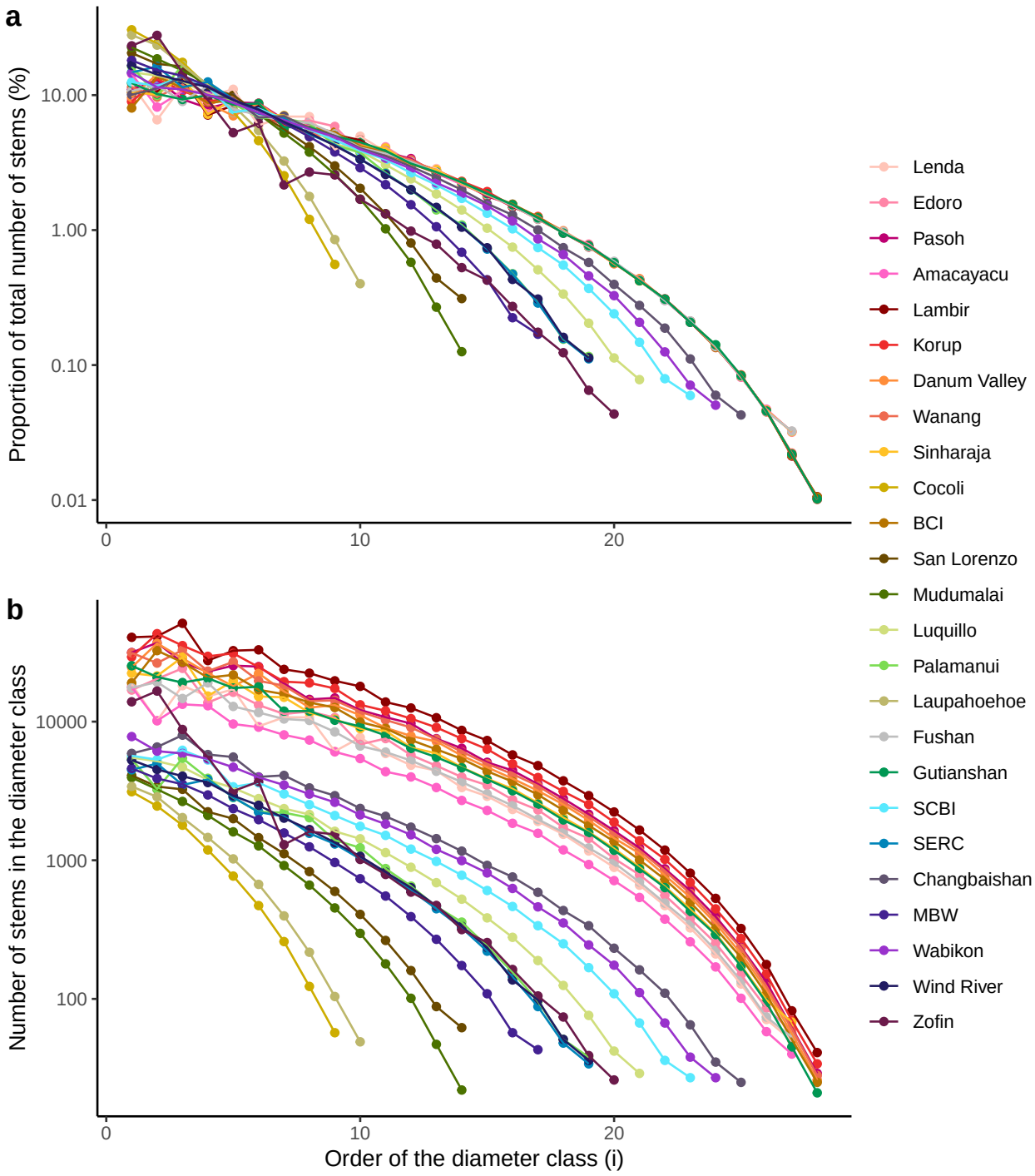

Figure S4: Definition of diameter classes per site. (a) Proportion and (b) number of stems per diameter class (ordered by DBH), in each site. Sites are listed in order of absolute latitude in the legend, and are colored in warm colors (red to green) for tropical sites, and in cold colors (green to blue) for temperate sites, as in the main text Figure 1.

Appendix D - Multiple linear regressions - climate effects

Table S4: Estimated effects of the multiple linear regressions of the median, dispersion (i.e. the quartile coefficient of dispersion) and skewness of aboveground biomass (AGB), aboveground woody productivity (AWP) and aboveground woody mortality (AWM) with mean annual temperature (MAT) and mean annual precipitation (MAP). The maximum-likelihood values of the coefficients are provided with the associated standard errors and p-values, as well as the multiple R-squared values for each linear regression.

Summary statistic	Biomass stock or flux	Coefficient	Estimate	Standard error	p-value	R-squared
median	AGB	Intercept	5.50e+01	5.4297994	0.000	0.002
		MAP	-6.44e-04	-0.1909188	0.850	
		MAT	2.78e-03	0.0049807	0.996	
	AWP	Intercept	5.39e+01	6.3831279	0.000	0.079
		MAP	-1.50e-03	-0.5349497	0.598	
		MAT	-3.68e-01	-0.7891584	0.438	
	AWM	Intercept	5.47e+01	4.5372464	0.000	0.006
		MAP	-7.59e-04	-0.1890639	0.852	
		MAT	-1.10e-01	-0.1659722	0.870	
dispersion	AGB	Intercept	1.26e-01	4.2991719	0.000	0.778
		MAP	2.44e-05	2.4939959	0.021	
		MAT	9.45e-03	5.8190230	0.000	
	AWP	Intercept	2.07e-01	4.9945002	0.000	0.603
		MAP	3.60e-06	0.2620016	0.796	
		MAT	1.09e-02	4.7654101	0.000	
	AWM	Intercept	2.78e-01	5.2188857	0.000	0.293
		MAP	7.00e-06	0.3969997	0.695	
		MAT	6.85e-03	2.3319956	0.029	
skewness	AGB	Intercept	-6.00e-02	-1.2822200	0.213	0.427
		MAP	3.42e-05	2.1908241	0.039	
		MAT	4.48e-03	1.7334312	0.097	
	AWP	Intercept	-1.38e-01	-2.7345523	0.012	0.588
		MAP	4.39e-05	2.6041395	0.016	
		MAT	7.91e-03	2.8308999	0.010	
	AWM	Intercept	-1.91e-02	-0.2391698	0.813	0.174
		MAP	2.30e-05	0.8669784	0.395	
		MAT	5.33e-03	1.2108598	0.239	

Table S5: Estimated effects of the multiple linear regressions of the median, dispersion (i.e. the quartile coefficient of dispersion) and skewness of aboveground biomass (AGB), aboveground woody productivity (AWP) and aboveground woody mortality (AWM) with mean annual temperature (MAT) and Selyaninov Hydrothermal Coefficient (SHC). SHC takes into account the effect of temperature on evapotranspiration. SHC values were extracted from a 1-km resolution raster downloaded from the CHELSA database (Karger et al., 2017; https://chelsa-climate.org/). The maximum-likelihood values of the coefficients are provided with the associated standard errors and p-values, as well as the multiple R-squared values for each linear regression. The effect of SHC (from CHELSA) on AGB stocks and fluxes distribution is qualitatively similar to the effect of MAP (from data provided by each site), but generally less significant.

Summary statistic	Biomass stock or flux	Coefficient	Estimate	Standard error	p-value	R-squared
median	AGB	Intercept	50.30000	3.5486821	0.002	0.0086519
		MAT	-0.06680	-0.1408455	0.889	
		SHC	1.24000	0.4232170	0.676	
	AWP	Intercept	52.60000	4.4094282	0.000	0.0669172
		MAT	-0.50100	-1.2554176	0.222	
		SHC	0.10000	0.0407901	0.968	
	AWM	Intercept	52.50000	3.1020960	0.005	0.0053363
		MAT	-0.18200	-0.3218606	0.751	
		SHC	0.49200	0.1408436	0.889	
dispersion	AGB	Intercept	0.08350	1.9240843	0.067	0.7542979
		MAT	0.01140	7.8615792	0.000	
		SHC	0.01680	1.8778321	0.074	
	AWP	Intercept	0.19900	3.4108421	0.003	0.6033604
		MAT	0.01120	5.7498165	0.000	
		SHC	0.00314	0.2611482	0.796	
	AWM	Intercept	0.24500	3.3080357	0.003	0.3035060
		MAT	0.00736	2.9658951	0.007	
		SHC	0.01060	0.6939677	0.495	
skewness	AGB	Intercept	-0.08640	-1.2143174	0.238	0.3294723
		MAT	0.00733	3.0820645	0.005	
		SHC	0.01380	0.9418317	0.357	
	AWP	Intercept	-0.19200	-2.4785747	0.021	0.5089609
		MAT	0.01150	4.4385457	0.000	
		SHC	0.02350	1.4686036	0.156	
	AWM	Intercept	-0.04920	-0.4353262	0.668	0.1570847
		MAT	0.00721	1.9079886	0.070	
		SHC	0.01290	0.5521822	0.586	

Table S6: Results of Wilcoxon rank-sign test for the difference between tropical and temperate plots in terms of the median, dispersion (i.e. the quartile coefficient of dispersion) and skewness of aboveground biomass (AGB), aboveground woody productivity (AWP) and aboveground woody mortality (AWM). The w-test statistics are provided with the associated p-values.

Summary statistic	Biomass stock or flux	w-test statistic	p-value
median	AGB	60	0.662
	AWP	42	0.137
	AWM	55	0.466
dispersion	AGB	131	0.000
	AWP	124	0.000
	AWM	125	0.000
skewness	AGB	120	0.001
	AWP	119	0.002
	AWM	106	0.027

Appendix E - Importance of large trees in AGB dynamics

Table S7: DBH threshold per site (cm), for the alternative definitions of large trees. Sites are listed in order of absolute latitude. Trees were considered to be in the large tree size class if their DBH was equal to or greater than this value.

Site	Top 5% of stems	Top 50% AGB
Lenda	75.900	71.50
Edoro	57.300	58.80
Pasoh	45.900	45.30
Amacayacu	45.624	38.54
Lambir	57.655	59.20
Korup	46.525	45.70
Danum Valley	52.681	77.90
Wanang	50.700	48.70
Sinharaja	54.100	47.50
Cocoli	82.520	79.40
BCI	57.562	59.79
San Lorenzo	52.304	50.30
Mudumalai	59.300	48.10
Luquillo	42.000	43.10
Palamanui	20.500	13.60
Laupahoehoe	66.520	63.30
Fushan	45.600	37.20
Gutianshan	40.240	30.50
SCBI	69.350	59.80
SERC	77.600	65.40
Changbaishan	63.200	53.50
MBW	55.200	46.50
Wabikon	39.700	31.70
Wind River	101.675	91.30
Zofin	86.000	78.00

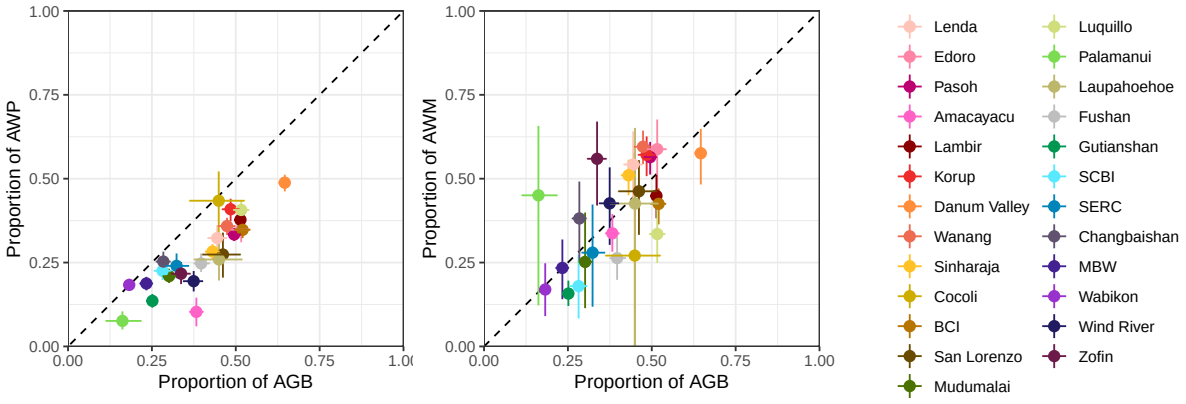

Figure S5: Proportions of AGB stocks and fluxes in large trees, when defined as the 5% largest stems in each site. Error bars represent the 95% confidence interval after bootstrapping 20 x 20 m quadrats with 1000 replicates. Dashed lines correspond to the y=x line. Sites are listed in order of absolute latitude in the legend, and are colored in warm colors (red to green) for tropical sites, and in cold colors (green to blue) for temperate sites.

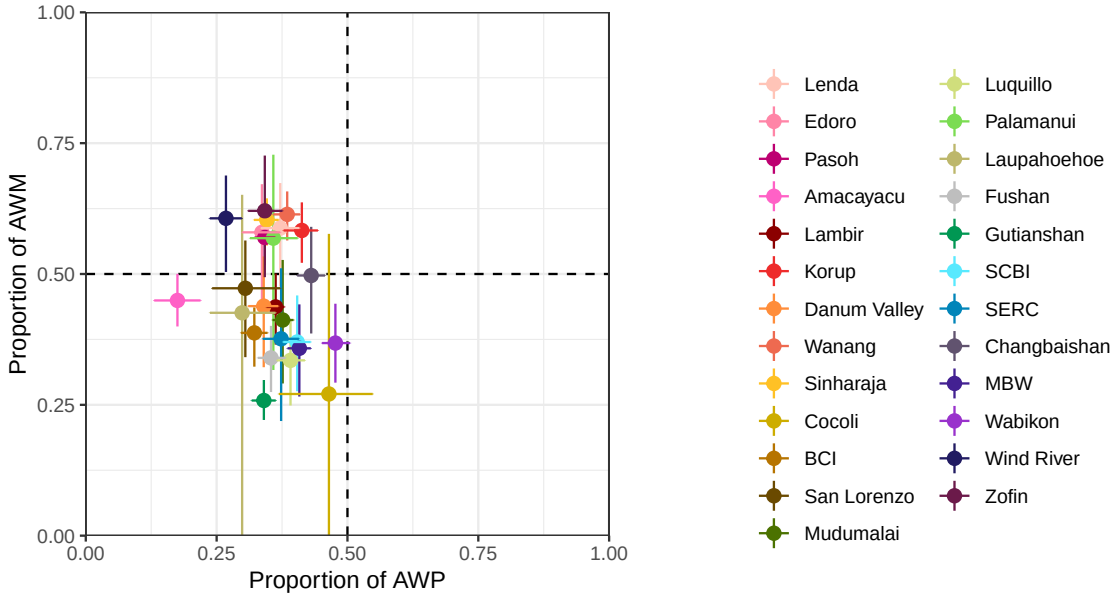

Figure S6: Proportion of AGB fluxes in large trees, when defined as the largest trees comprising 50% of total AGB in each site. Error bars represent the 95% confidence interval after bootstrapping 20 x 20m quadrats with 1000 replicates. Dashed lines correspond to the x = 0.5 and y = 0.5 lines (matching the proportion of AGB in large trees, by definition).

Appendix F - Additional variables

Notes S1

The distribution of AGB with tree diameter depends fundamentally on the numbers of trees of different diameters and on how individual tree biomass varies with stem diameter (Figure S7). The tree diameter distributions differ in shape between temperate and tropical sites (Figure S7a): in temperate sites the distributions are more strongly curved downwards towards lower abundance as stem diameter increases, whereas in tropical sites they are closer to power functions (straight lines on log-log axis). In contrast, tree biomass is almost exactly a power function of diameter in all sites (biomass increasing as stem diameter increases). In tropical sites there are only minor deviations reflecting differences in mean wood densities with diameter. In temperate sites, where we used genus-specific biomass equations that do not explicitly include wood density (Chojnacky *et al.*, 2014), deviations from a power function are due to differences in species composition and associated biomass equations (Figure S7b). Thus, variation in the distribution of AGB parallels variation in tree size distributions (Figure S7c), with temperate sites' AGB peaking for medium to large stems and decreasing abruptly for larger stems, whereas AGB is more homogeneously distributed across diameter classes in tropical sites.

The tree diameter distribution (Figure S7a) in combination with variation in growth and thus productivity per tree with diameter (Figure S8a) determines the distribution of AWP with diameter (Figure S8b).

Stem mortality rates generally decrease with tree size at most sites (Figure S9a). However, a few sites exhibit U-shaped patterns, with lowest mortality rates for intermediate size classes. Mortality patterns are relatively noisy, especially at large size classes, reflecting the binomial nature of the process and the relatively small sample sizes for large trees. These mortality rate patterns together with tree diameter distributions (Figure S7a) determine the distribution of AWM with size (Figure S9b).

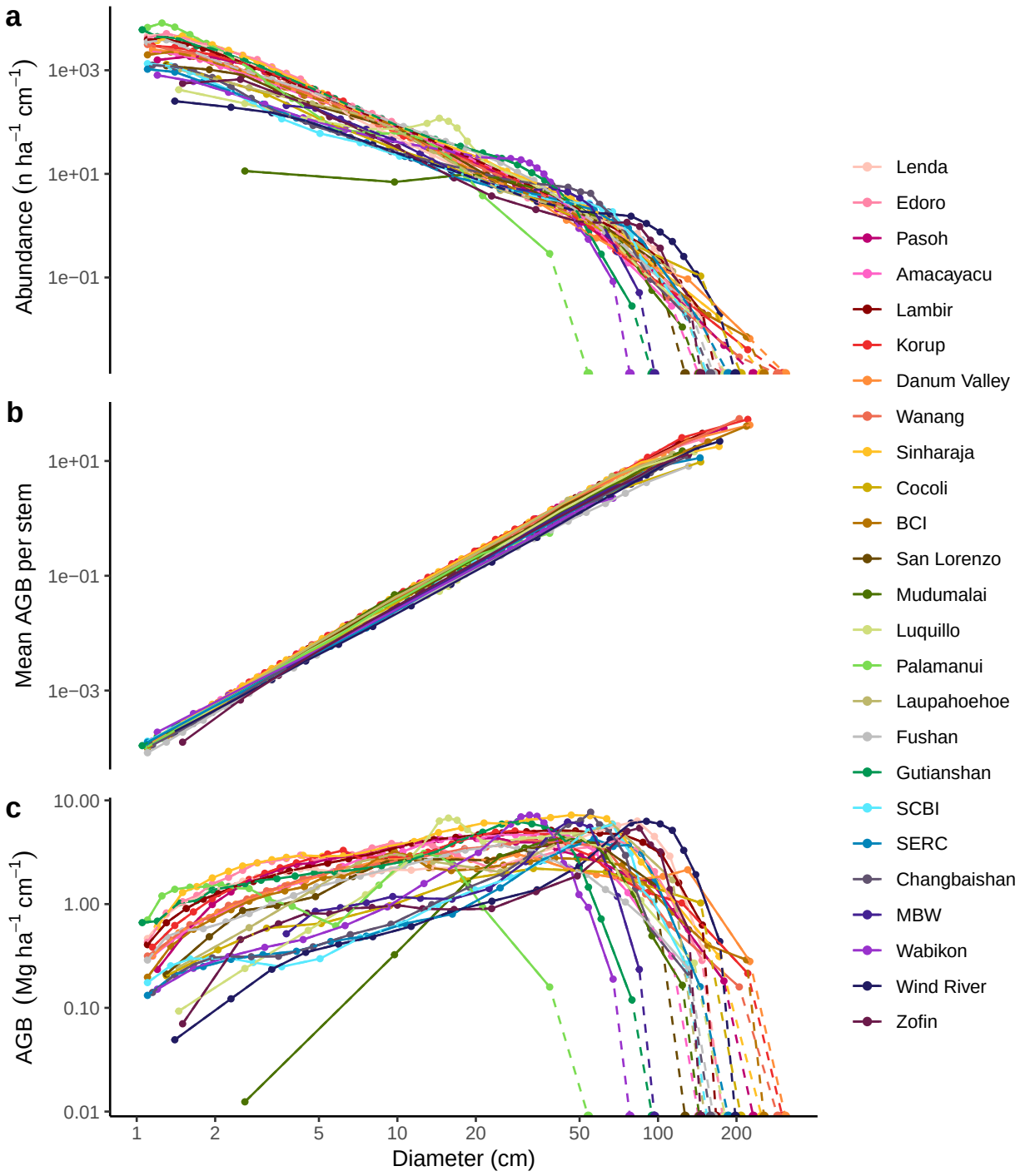

Figure S7: Size-related variation in (a) stem density (n.ha^{-1}.cm^{-1}), (b) mean individual stem aboveground biomass, and (c) total aboveground live biomass (AGB, Mg ha^{-1} cm^{-1}) in the focal forests. Note that axes are log-scaled (panel c displays the same data as main text Figure 1a,b, but differs in the axis scaling and in that the main text figure is of the probability density). Sites are listed by increasing absolute latitude, which is also indicated by a shift in colors from red (tropical) to dark blue (boreal). The last points of each curve in panels (a) and (c), placed on the x-axis, represent the end of the distribution, i.e. the size of the largest tree in each site.

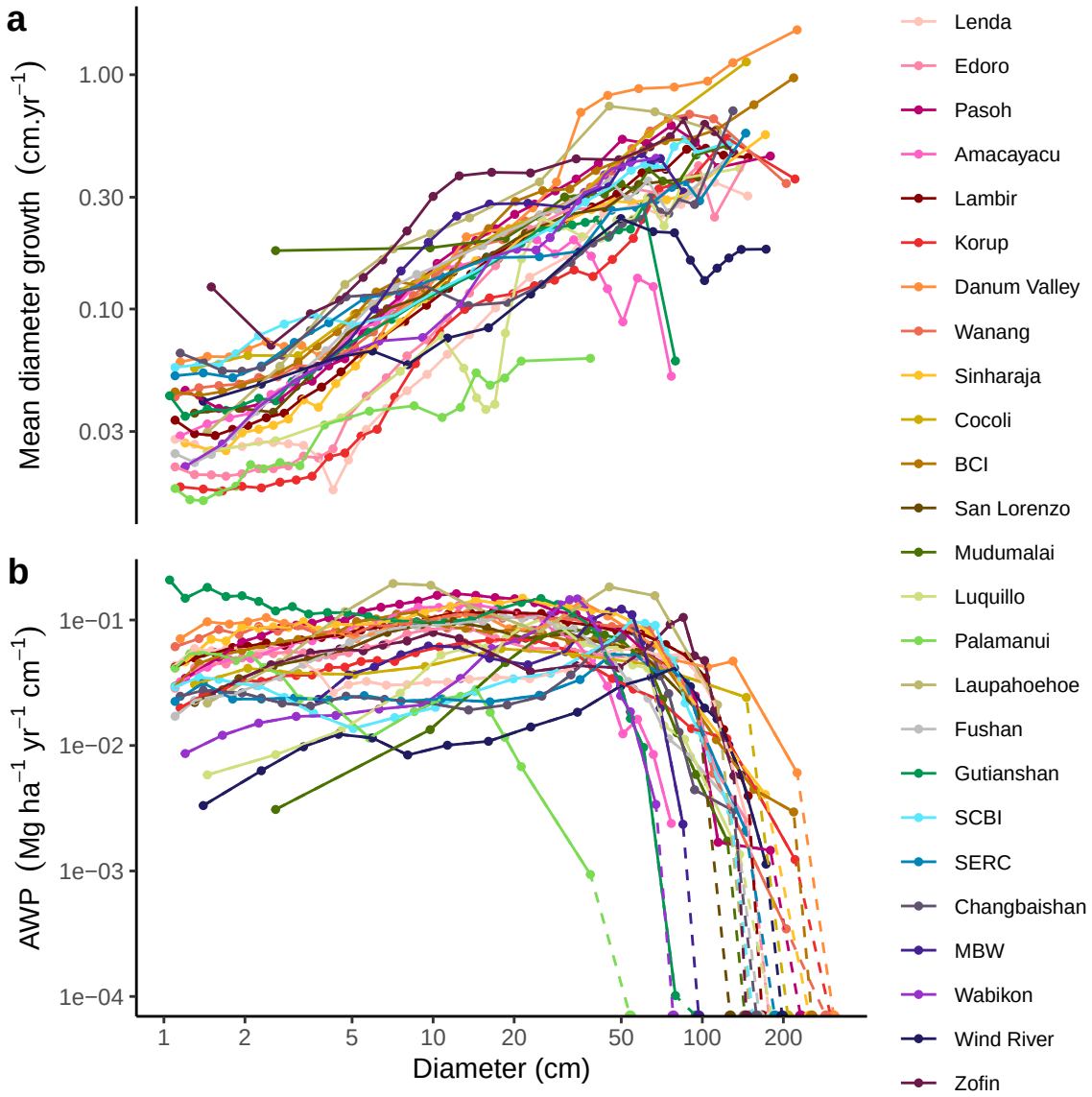

Figure S8: Size-related variation in (a) mean stem diameter growth (cm.yr^{-1}), and (b) total aboveground woody productivity (AWP, Mg ha^{-1} yr^{-1} cm^{-1}). Note that axes are log-scaled (panel b displays the same data as main text Figure 1d,e, but differs in the axis scaling and in that the main text figure is of the probability density). Sites are listed by increasing absolute latitude, which is also indicated by a shift in colors from red (tropical) to dark blue (boreal). The last points of each curve in panel (b), placed on the x-axis, represent the end of the distribution, i.e. the size of the largest tree in each site.

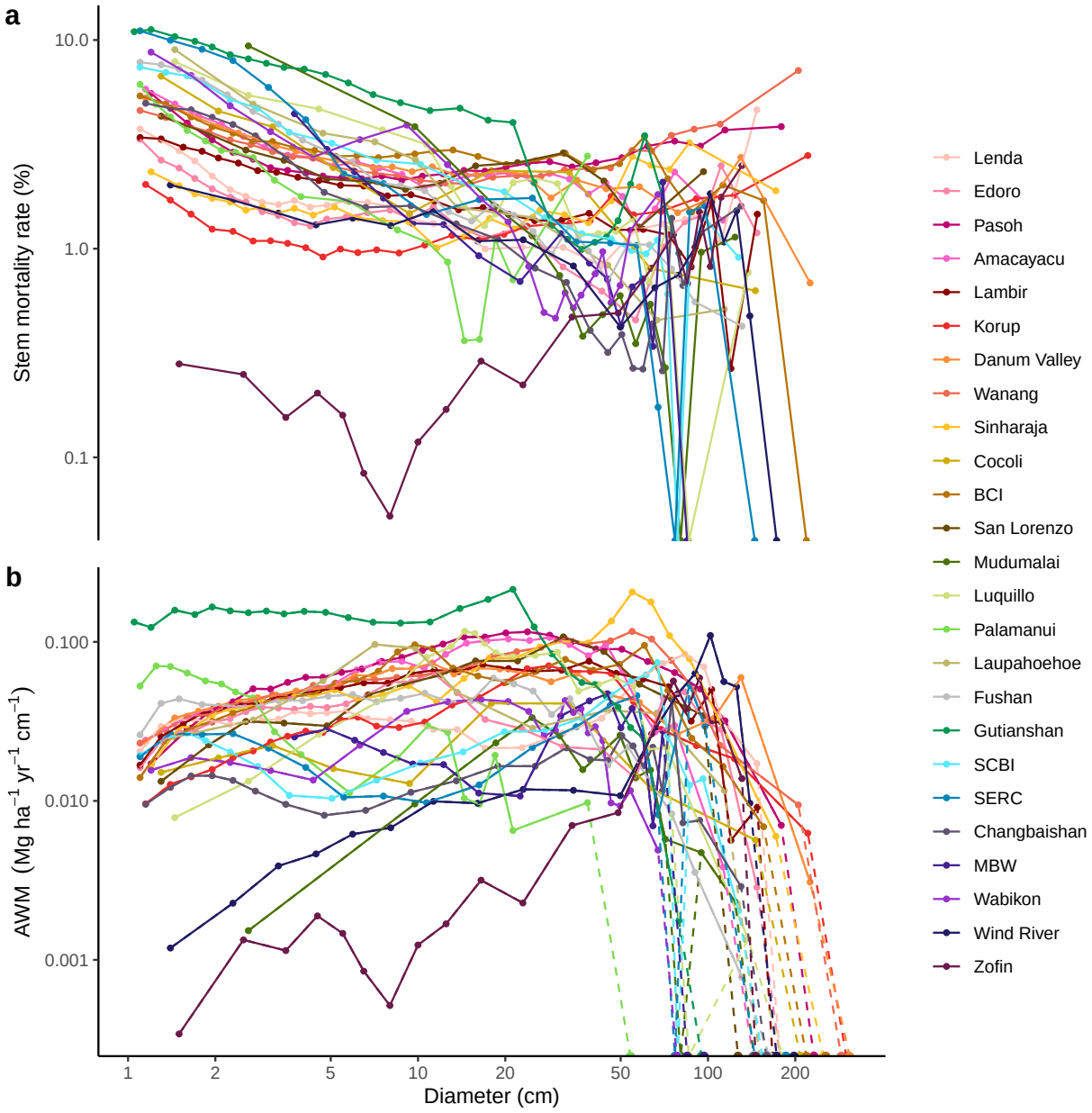

Figure S9: Size-related variation in (a) stem mortality rate (% yr^{-1}) and (b) total aboveground woody mortality (AWM, Mg ha^{-1} yr^{-1} cm^{-1}). Note that axes are log-scaled (panel b displays the same data as main text Figure 1g,h, but differs in the axis scaling and in that the main text figure is of the probability density). Sites are listed by increasing absolute latitude, which is also indicated by a shift in colors from red (tropical) to dark blue (boreal). The last points of each curve in panel (b), placed on the x-axis, represent the end of the distribution, i.e. the size of the largest tree in each site.

Appendix G - Size distributions of AGB stocks and fluxes per site

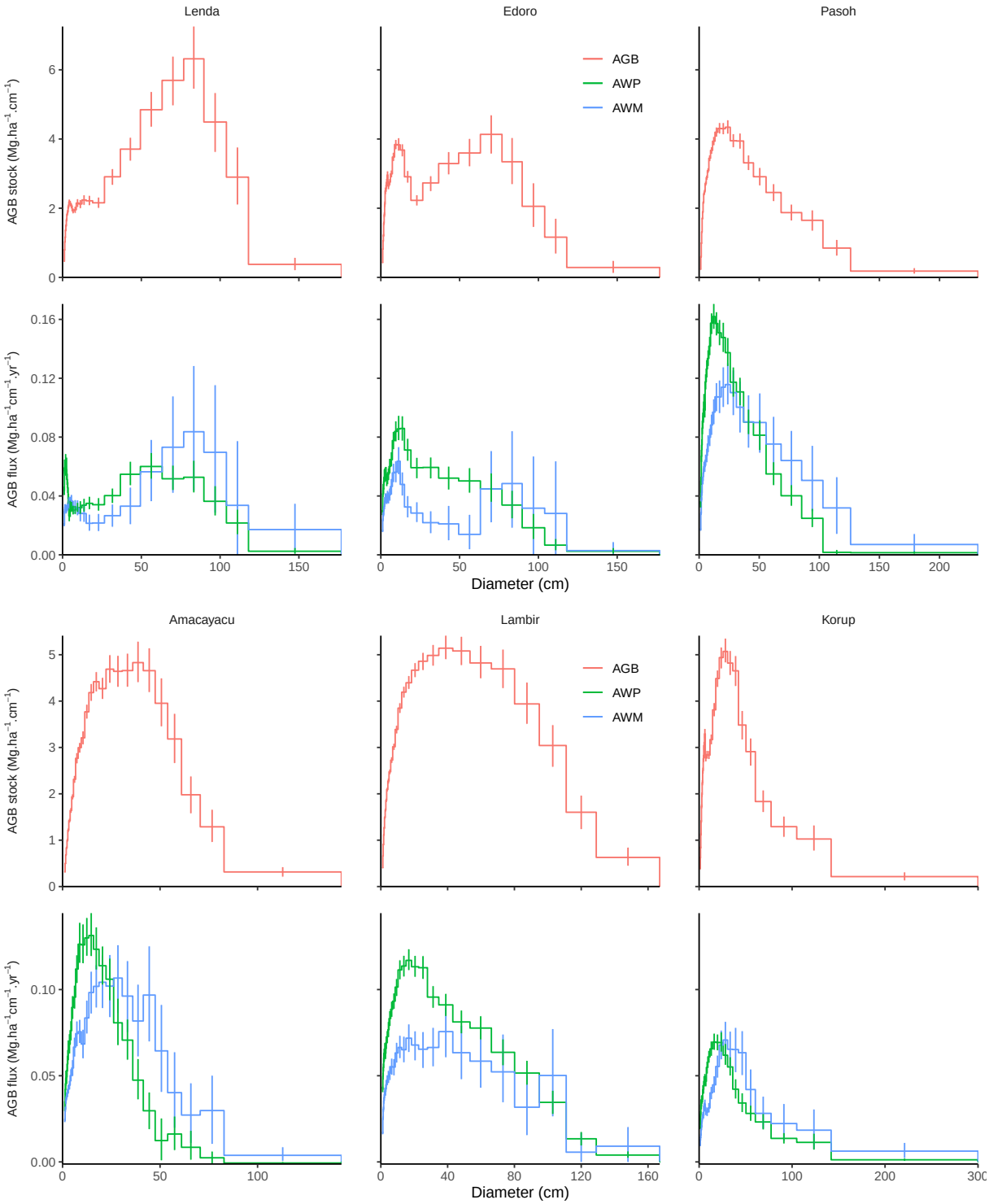

Figure S10: AGB stocks (top panels, red) and fluxes (AWP in green, AWM in blue, lower panels) per site. Sites are listed by absolute latitude. Error bars represent the 95% confidence interval after bootstrapping 20 x 20m quadrats with 1000 replicates.

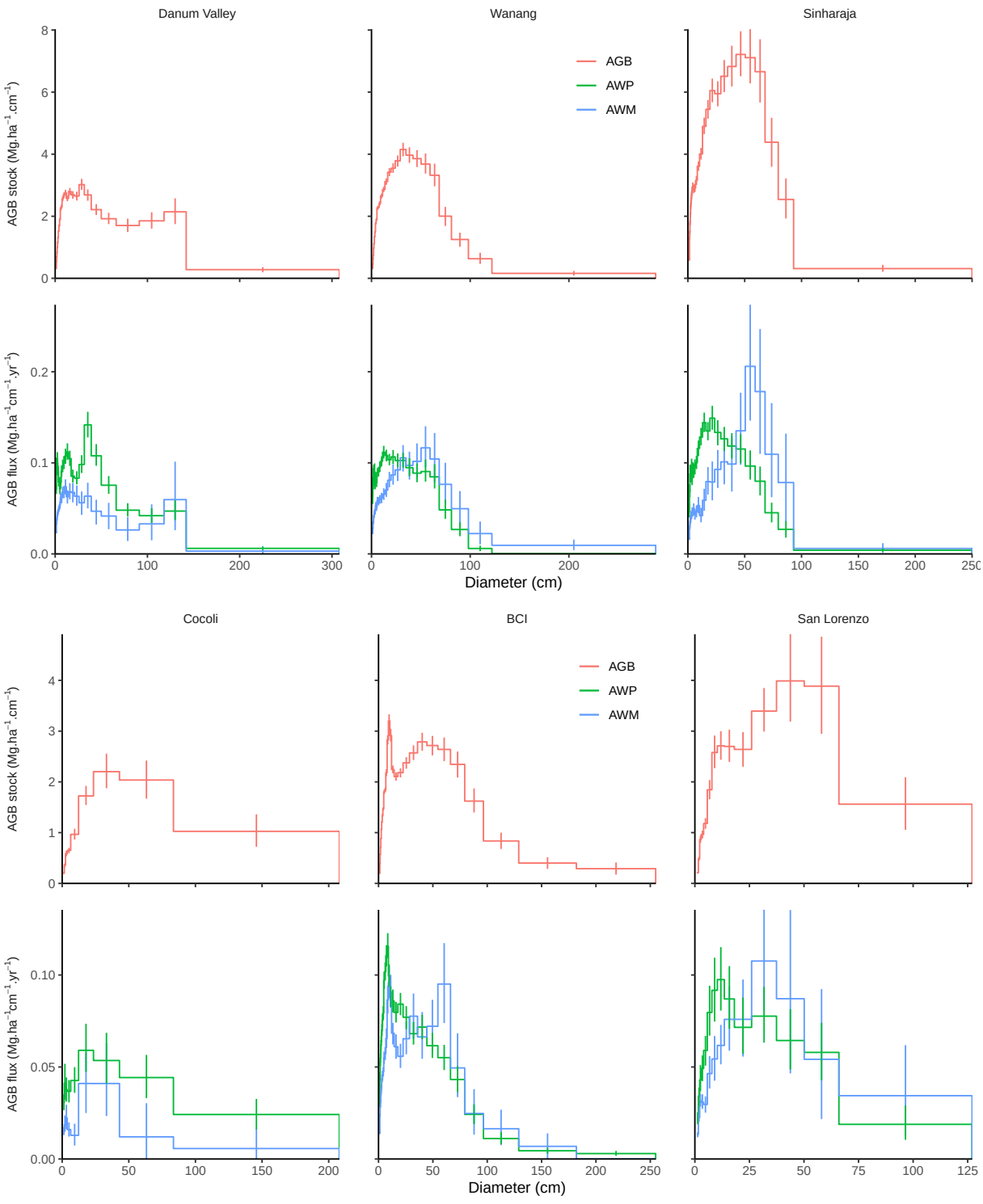

Figure S10 continued

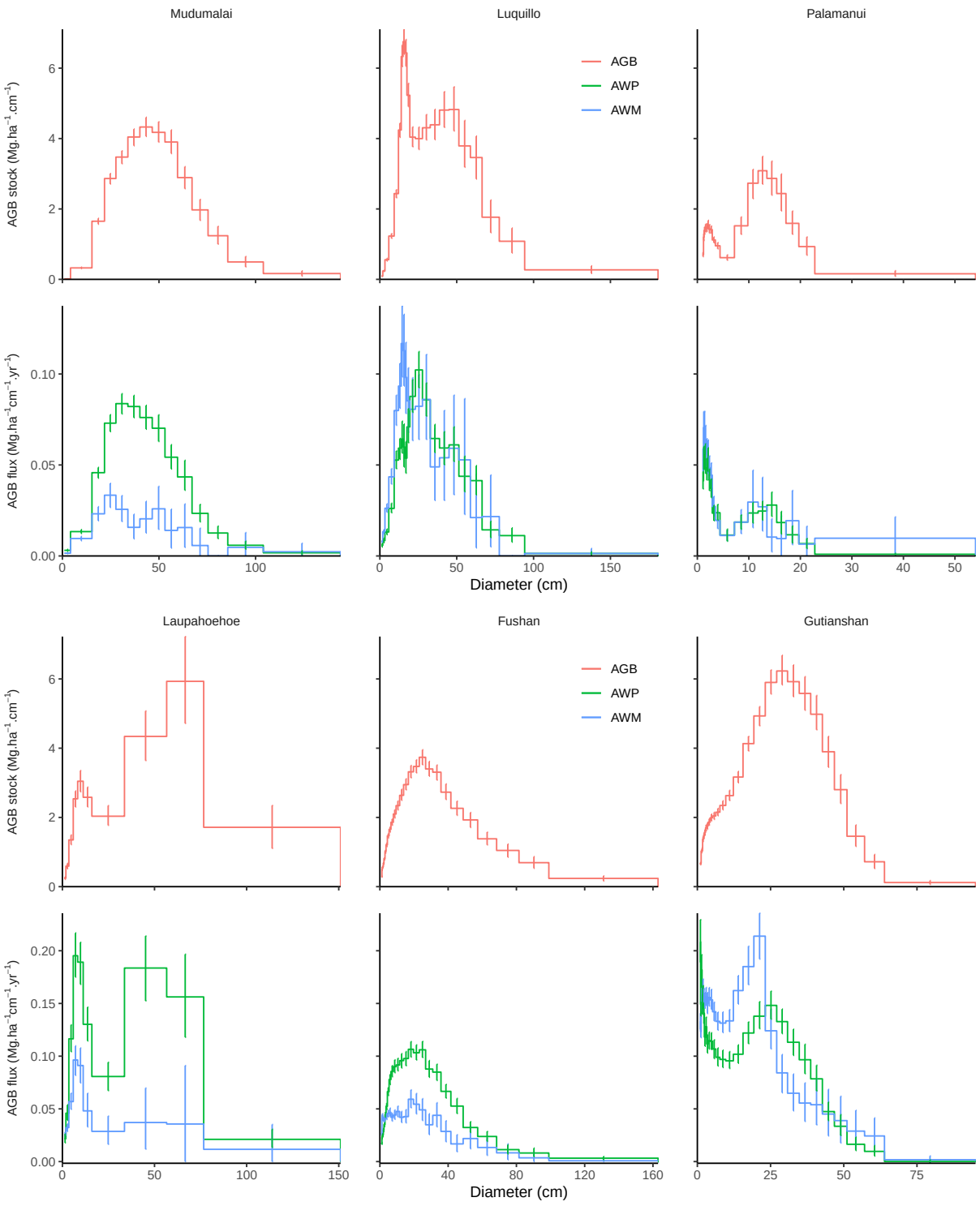

Figure S10 continued

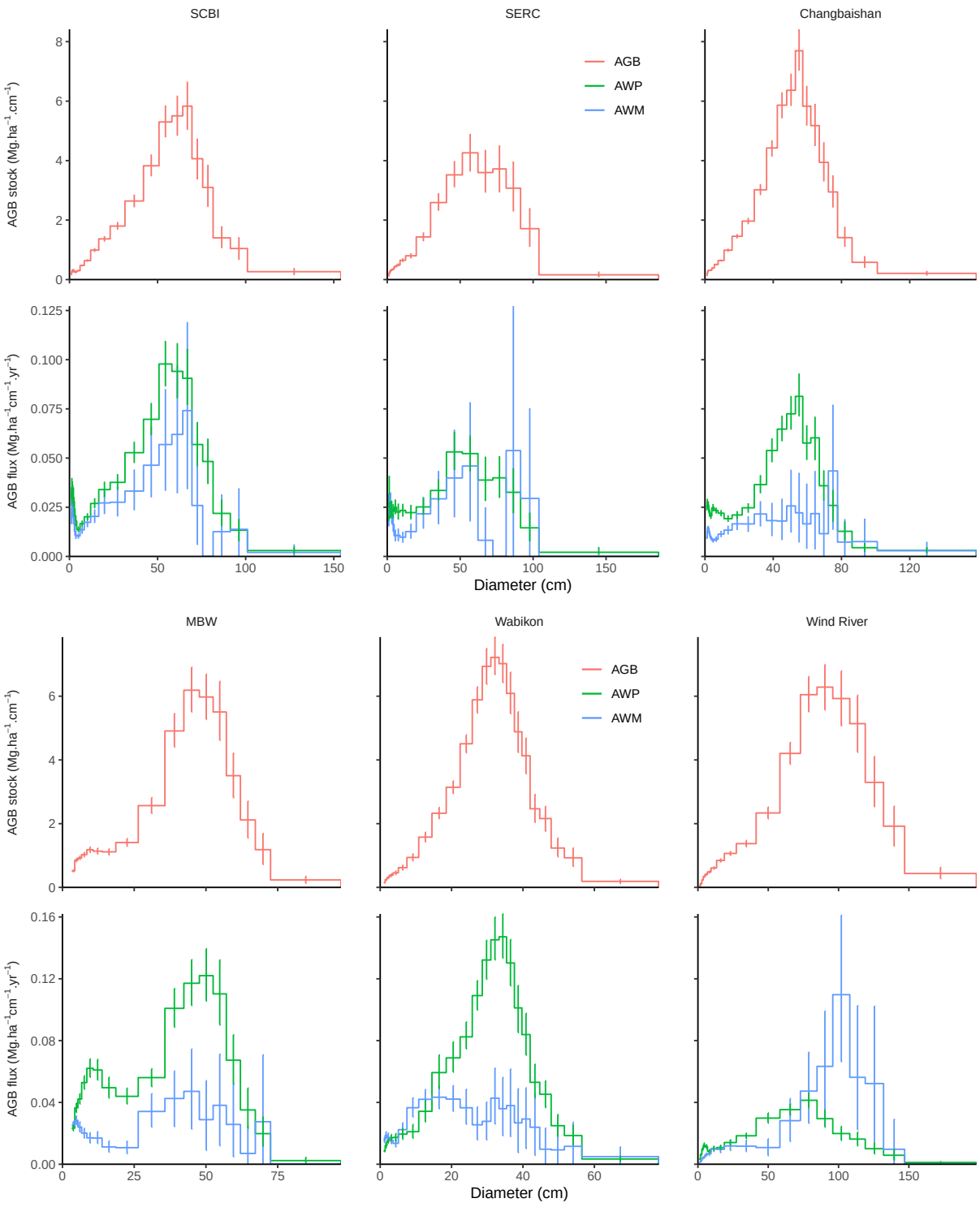

Figure S10 continued

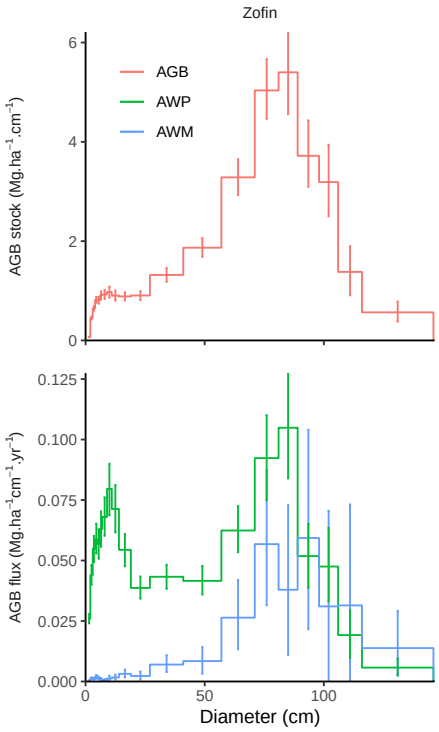

Figure S10 continued

Appendix H - Complete figures including Palamanui site

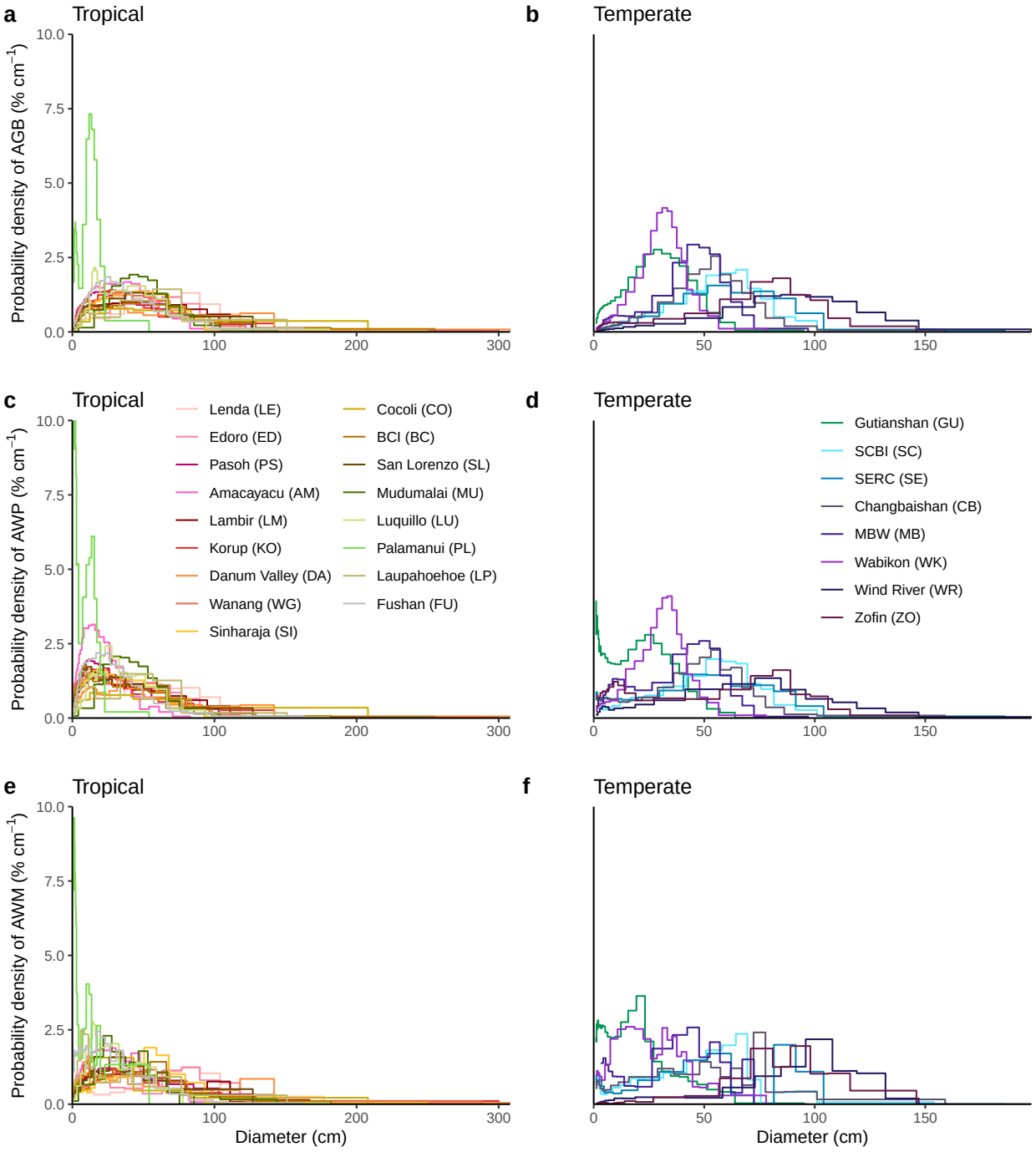

Figure S11: Size-related distributions (% cm^{-1}) of above-ground biomass (AGB, in panels a, b), aboveground woody productivity (AWP, panels c,d), and aboveground woody mortality (AWM, panels e,f) in tropical (a,c,e) and temperate (b,d,f) sites. Diameter classes for plotting vary among sites depending on the number and size distribution of stems (Appendix B). Medians are defined as the diameters at which 50% of the stock or flux is in smaller stems. The legend (c,d) lists sites by absolute latitude. This figure is the untruncated version of Fig. 1 of the manuscript (including Palamanui, a dry forest with a large proportion of small stems).

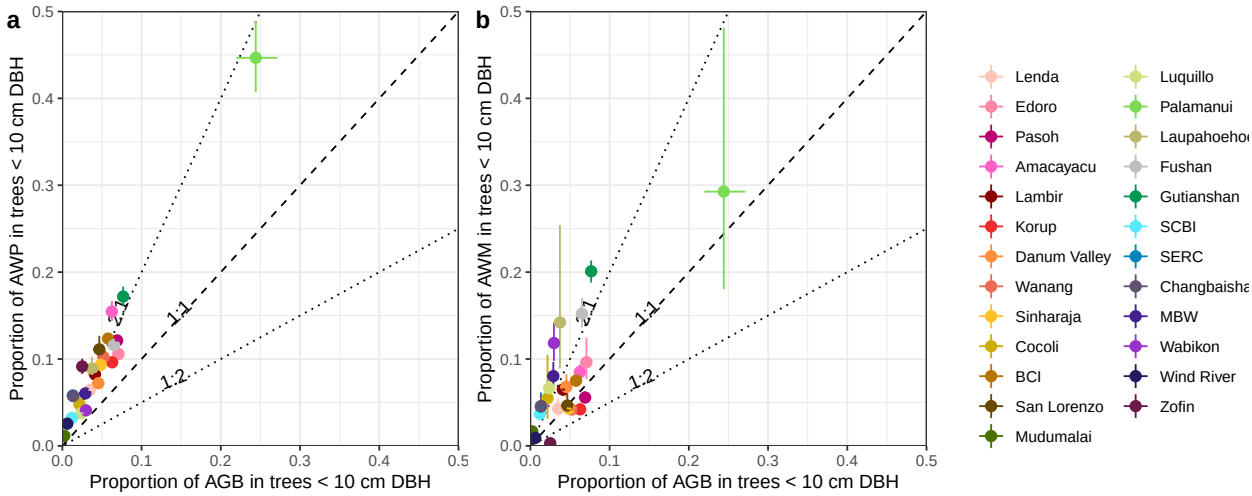

Figure S12: Proportion of carbon stocks and fluxes in small trees. Error bars represent 95% CIs after bootstrapping over 20 x 20 m quadrats with 1000 replicates. Dashed lines correspond to (starting from the top): y = 2x, y = x, and y = x/2. This figure is the untruncated version of Fig. 4 of the manuscript (including Palamanui, a dry forest with a large proportion of small stems).

Appendix I - Site-specific acknowledgments

Notes S2

Amacayacu The 25-ha Long-Term Ecological Research Project of Amacayacu is a collaborative project of the Instituto Amazónico de Investigaciones Científicas Sinchi and the Universidad Nacional de Colombia Sede Medellín, in partnership with the Unidad de Manejo Especial de Parques Naturales Nacionales and the Center for Tropical Forest Science of the Smithsonian Tropical Research Institute (CTFS). We acknowledge the Director and staff of the Amacayacu National Park for supporting and maintaining the project in this National Park, as well as coworkers in the Comunidad Indígena Palmeras for their assistance in collecting the tree census data.

Barro Colorado Island The BCI forest dynamics research project was made possible by National Science Foundation grants to Stephen P. Hubbell: DEB-0640386, DEB-0425651, DEB-0346488, DEB-0129874, DEB-00753102, DEB-9909347, DEB-9615226, DEB-9615226, DEB-9405933, DEB-9221033, DEB-9100058, DEB-8906869, DEB-8605042, DEB-8206992, DEB-7922197, support from the Center for Tropical Forest Science, the Smithsonian Tropical Research Institute, the John D. and Catherine T. MacArthur Foundation, the Mellon Foundation, the Small World Institute Fund, numerous private individuals, and through the hard work of over 100 people from 10 countries over the past two decades.

Changbaishan Zhanqing Hao and Xugao Wang were supported by The National Key Research and Development Program of China (2016YFC0500302), National Natural Science Foundation of China (31570432 and 31370444), Key Research Program of Frontier Sciences, CAS (QYZDB-SSW-DQC002).

Cocoli The 4-ha Cocoli forest dynamics plot is supported by the Smithsonian Tropical Research Institute. Thank you to the plot Principal Investigators Richard Condit, Rolando Pérez, and Salomón Aguilar, and many field workers, students, technicians, and STRI staff.

Danum Valley The Danum plot is a core project of the Southeast Asia Rain Forest Research Partnership (SEARRP). We thank SEARRP partners especially Yayasan Sabah for their support, and HSBC Malaysia and the University of Zurich for funding. We are grateful to the research assistants who are conducting the census, in particular the team leader Alex Karolus, and to Mike Bernados and Bill McDonald for species identifications. We thank Stuart Davies and Shameema Esufali for advice and training.

Fushan Taiwan Forestry Bureau, Taiwan Forestry Research Institute, National Taiwan University (Institute of Ecology and Evolutionary Biology), and the Center for Tropical Forest Science of the Smithsonian Tropical Research Institute.

Gutianshan We thank Drs. Mingjian Yu from Zhejiang University, Jianhua Chen for their contributions to the establishment and census of the 24-ha permanent forest plot. We gratefully acknowledge support from the Administration Bureau of the Gutianshan National Nature Reserve.

Ituri (Edoro and Lenda) The Ituri 40-ha plot program is a collaborative project between the Centre de Formation et de Recherche en Conservation Forestière, the Wildlife Conservation Society – DRC through his conservation project in the Okapi Forest Reserve, in partnership with the Center for Tropical Forest Science of the Smithsonian Tropical Research Institute. The Ituri plots are financially supported by the Wildlife Conservation Society, the Frank Levinson Family Foundation, and the Smithsonian Forest Global Earth Observatory. The Institut Congolais pour la Conservation de la Nature graciously provided the research permit.

Korup The 50-ha Korup Forest Dynamics Plot is affiliated with the Smithsonian's Center for Tropical Forest Science - Forest Global Earth Observatory. The 3 principal investigators gratefully acknowledge funding and other support received from CTFS for our first and secondcensuses. Funding from the Botanical Research Foundation of Idaho is also gratefully acknowledged. Permission to conduct the field program in Cameroon is provided by the Ministry of Environment and Forests and the Ministry of Scientific Research and Innovation. We also acknowledge the dedicated support of our field team, especially field leadership by Sainge Nsanyi Moses and botanical work by Ekole Mambo Peter.

Lambir The 52-ha Long-Term Ecological Research Project is a collaborative project of the Forest Department

of Sarawak, Malaysia, the Center for Tropical Forest Science of the Smithsonian Tropical Research Institute, the Arnold Arboretum of Harvard University, USA (under NSF awards DEB-9107247 and DEB-9629601), and Osaka City, Ehime & Kyoto Universities, Japan (under MEXT/JSPS grants 09NP0901, 17H04602 and JST/JICA-SATREPS). The Lambir Forest Dynamics Plot is part the Center for Tropical Forest Science, a global network of large-scale demographic tree plots. We acknowledge the Sarawak Forest Department for supporting and maintaining the project in Lambir Hills National Park.

Laupahoehoe and Palamanui This work is possible because of support provided by NSF EPSCoR (Grant Numbers EPS- 0554657 and EPS-0903833), the USDA Forest Service, the University of Hawaii, and the University of California at Los Angeles. We thank the USDA Forest Service and State of Hawaii Department of Land and Natural Resources Division of Forestry and Wildlife for access to the Hawaii Experimental Tropical Forest. For Palamanui we acknowledge the Hunt Companies, especially Roger Harris, for access to this lowland dry forest site.

Luquillo This work would not have been possible without the $>$ 100 volunteers and staff that have assisted in the tree censuses of the Luquillo Forest Dynamic Plot (LFDP). We thank the information management team in the Luquillo LTER office and the El Verde Field Station staff for their hard work and support. This research was supported by grants BSR-8811902, DEB 9411973, DEB 0080538, DEB 0218039, DEB 0620910, DEB 0963447, DEB-129764, DEB-1546686 AND DEB-1831952 from NSF to the Department of Environmental Science, University of Puerto Rico, and to the International Institute of Tropical Forestry, USDA Forest Service, as part of the Luquillo Long-Term Ecological Research Program. The U.S. Forest Service (Dept. of Agriculture) and the University of Puerto Rico gave additional support. The LFDP has also been supported by the Andrew Mellon foundation and the Smithsonian Institution Forest Global Earth Observatory.

Michigan Big Woods We would like to thank the University of Michigan and Middlebury College students who have helped with all of the censuses of the Big Woods Plot. These censuses were supported by the Edwin S. George Reserve Fund, a USDA McIntyre-Stennis Grant, and the Middlebury College Millennium Fund.

Mudumalai Funding was received from the Ministry of Environment, Forest and Climate Change, Government of India and the Department of Biotechnology, Government of India. R Sukumar was a JC Bose National Fellow during the tenure of this work.

Pasoh Data from the Pasoh Research Forest was provided by the Forest Research Institute Malaysia-Forest Global Earth Observatory, Smithsonian Tropical Research Institute collaborative research project. Negeri Sembilan Forestry Department is the custodian of Pasoh Research Forest and we acknowledge the department for preserving the research forest.

San Lorenzo The 5.96-ha San Lorenzo forest dynamics plot is supported by the Smithsonian Tropical Research Institute. Thank you to the plot Principal Investigators Richard Condit, Rolando Pérez, and Salomón Aguilar, and many field workers, technicians, and STRI staff.

SCBI Funding for the Smithsonian Conservation Biology Institute (SCBI) large forest dynamics plot was provided by the Smithsonian Institution (Forest Global Earth Observatory and the National Zoological Park, and the HSBC Climate Partnership.

SERC Smithsonian Environmental Research Center, Earthwatch Institute Tyson: The Tyson Research Center Forest Dynamics Plot (TRCP) is supported by Washington University in St. Louis' Tyson Research Center. Funding was provided by the International Center for Advanced Renewable Energy and Sustainability (I-CARES) at Washington University in St. Louis, the National Science Foundation (DEB 1557094), and the Tyson Research Center. We thank the Tyson Research Center staff for providing logistical support, and the more than 100 high school students, undergraduate students, and researchers that have contributed to the project. The TRCP is part of the Center for Tropical Forest Science-Forest Global Earth Observatory (CTFS-ForestGEO), a global network of large-scale forest dynamics plots.

Sinharaja The authors gratefully acknowledge the permission given to work in Sinharaja World Heritage Site by the Forest Department of Sri Lanka, as well as the generous financial assistance given to set up the plot and for censuses by the Forest Global Earth Observatory (ForestGEO) of the Smithsonian Tropical

Research Institute. We gratefully acknowledge logistical support from Uva Wellassa University, University of Peradeniya and Yale University.

Wabikon The Wabikon Lake Forest Dynamics Plot, located in the Chequamegon-Nicolet National Forest of northern Wisconsin, is part of the Smithsonian Institution's CTFS-ForestGEO network. Tree censuses at the site have been supported by the 1923 Fund, the Smithsonian Tropical Research Institute, and the Cofrin Center for Biodiversity at the University of Wisconsin-Green Bay. More than 50 scientists and student assistants contributed to the first two plot censuses. We are particularly grateful for the leadership of Gary Fewless, Steve Dhein, Kathryn Corio, Juniper Sundance, Cindy Burtley, Curt Rollman, Mike Stiefvater, Kim McKeefry, and U.S. Forest Service collaborators Linda Parker and Steve Janke.

Wanang The 50-ha Wanang Forest Dynamics Plot is a collaborative project of the New Guinea Binatang Research Center, the Center for Tropical Forest Science of the Smithsonian Tropical Research Institute, the Forest Research Institute of Papua New Guinea, the Czech Academy of Sciences and the University of Minnesota supported by NSF DEB-0816749 and the Czech Science Foundation 19-28126X. We acknowledge the government of Papua New Guinea and the customary landowners of Wanang for supporting and maintaining the plot.

Wind River The Wind River Forest Dynamics Plot is a collaborative project of Utah State University and the Utah Agricultural Experiment Station (Lutz *et al.*, 2013). Funding has been provided by the Center for Tropical Forest Science of the Smithsonian Tropical Research Institute, Utah State University, and the National Science Foundation (DEB #1542681). We acknowledge the Gifford Pinchot National Forest and the Wind River Field Station for providing logistical support, and the students, volunteers and staff individually listed at http://wfdp.org for data collection. The Wind River Forest Dynamics Plot was made possible by a grant from Jennifer Walston Johnson to the Smithsonian ForestGEO.

Zofin The Žofín Forest Dynamics Plot was established with the support of Smithsonian Institution; the long-term plot maintenance and monitoring is provided by the Department of Forest Ecology of the Silva Tarouca Research Institute, supported by the Czech Science Foundation (20-17282S). The Žofín Forest Dynamics Plot is part of the Center for Tropical Forest Science-Forest Global Earth Observatory (CTFS-ForestGEO), a worldwide network of large, long-term forest dynamics plots.

References

Allen D, Dick CW, Burnham RJ, Perfecto I, Vandermeer JH. **2019**. The Michigan Big Woods research plot at the Edwin S. George Reserve, Pinckney, MI, USA. *Miscellaneous publications of the Museum of Zoology, University of Michigan* **207**: 1–48.

Bourg NA, McShea WJ, Thompson JR, McGarvey JC, Shen X. **2013**. Initial census, woody seedling, seed rain, and stand structure data for the SCBI SIGEO Large Forest Dynamics Plot. *Ecology* **94**: 2111–2112.

Chen L, Mi X, Comita LS, Zhang L, Ren H, Ma K. **2010**. Community-level consequences of density dependence and habitat association in a subtropical broad-leaved forest. *Ecology Letters* **13**: 695–704.

Chojnacky DC, Heath LS, Jenkins JC. **2014**. Updated generalized biomass equations for North American tree species. *Forestry* **87**: 129–151.

Condit RS. **1998**. *Tropical forest census plots: methods and results from Barro Colorado Island, Panama and a comparison with other plots*. Berlin, Germany: Springer-Verlag.

Condit R, Aguilar S, Hernandez A, Perez R, Lao S, Angehr G, Hubbell SP, Foster RB. **2004**. Tropical forest dynamics across a rainfall gradient and the impact of an El Niño dry season. *Journal of Tropical Ecology* **20**: 51–72.

Condit R, Pérez R, Lao S, Aguilar S, Hubbell SP. **2017**. Demographic trends and climate over 35 years in the Barro Colorado 50 ha plot. *Forest Ecosystems* **4**: 1–13.

Enders RK. **1935**. Mammalian Life Histories from Barro Colorado Island, Panama. *Bulletin of the Museum of Comparative Zoology Harvard* **78**: 385–502.

Harms KE, Condit R, Hubbell SP, Foster RB, Harmst KE, Condit R, Hubbell SP, Fostert RB. **2001**. Habitat Associations of Trees and Shrubs in a 50-Ha Neotropical Forest Plot. *Journal of Ecology* **89**: 947–959.

Heijink BM, McMichael CNH, Piperno DR, Duivenvoorden JF, Cárdenas D, Duque Á. **2020**. Holocene increases in palm abundances in north-western Amazonia. *Journal of Biogeography* **47**: 698–711.

Hubbell SP, Foster RB, O'Brien ST, Harms KE, Condit R, Wechsler B, Wright SJ, Loo de Lao S. **1999**. Light-Gap Disturbances, Recruitment Limitation, and Tree Diversity in a Neotropical Forest. *Science* **283**: 554–557.

Inman-Narahari F, Giardina C, Ostertag R, Cordell S, Sack L. **2010**. Digital data collection in forest dynamics plots. *Methods in Ecology and Evolution* **1**: 274–279.

Janík D, Král K, Adam D, Hort L, Samonil P, Unar P, Vrska T, McMahon S. **2016**. Tree spatial patterns of Fagus sylvatica expansion over 37 years. *Forest Ecology and Management* **375**: 134–145.

Karger DN, Conrad O, Böhner J, Kawohl T, Kreft H, Soria-Auza RW, Zimmermann NE, Linder HP, Kessler M. **2017**. Climatologies at high resolution for the earth's land surface areas. *Scientific Data* **4**: 1–20.

Kenfack D, Thomas DW, Chuyong G, Condit R. **2007**. Rarity and abundance in a diverse African forest. *Biodiversity and Conservation* **16**: 2045–2074.

Kohyama TS, Kohyama TI, Sheil D. **2019**. Estimating net biomass production and loss from repeated measurements of trees in forests and woodlands: Formulae, biases and recommendations. *Forest Ecology and Management* **433**: 729–740.

Lee H, Davies SJ, LaFrankie JV, Tan S, Itoh A, Yamakura T, Ashton PS. **2002**. Floristic and structural diversity of 52 hectares of mixed dipterocarp forest in Lambir Hills National Park, Sarawak, Malaysia. *Journal of Tropical Forest Science* **14**: 379–400.

Lin TC, Hamburg SP, Lin KC, Wang LJ, Chang CT, Hsia YJ, Vadeboncoeur MA, McMullen CM, Liu CP. **2011**. Typhoon Disturbance and Forest Dynamics: Lessons from a Northwest Pacific Subtropical Forest. *Ecosystems* **14**: 127–143.

Lutz JA, Larson AJ, Freund JA, Swanson ME, Bible KJ. **2013**. The importance of large-diameter trees to forest structural heterogeneity. *PLoS ONE* **8**.

Makana J-R, C. Thomas S. **2004**. Dispersal limits natural recruitment of African mahoganies. *Oikos* **106**: 67–72.

Manokaran N, LaFrankie JV. **1990**. Stand Structure of Pasoh Forest Reserve, A lowland rainforest in Peninsular Malaysia. *Journal of Tropical Forest Science* **3**: 14–24.

Mcmahon SM, Parker GG. **2015**. A general model of intra-annual tree growth using dendrometer bands. *Ecology and Evolution* **5**: 243–254.

Nunes MH, Both S, Bongalov B, Brelsford C, Khoury S, Burslem DFRP, Philipson C, Majalap N, Riutta T, Coomes DA ***et al.*** **2019**. Changes in leaf functional traits of rainforest canopy trees associated with an El Nino event in Borneo. *Environmental Research Letters* **14**.

Su S-H, Hsieh C-F, Chang-Yang C-H, Lu C-L, Guan BT. **2010**. Micro-Topographic Differentiation of the Tree Species Composition in a Subtropical Submontane Rainforest in Northeastern Taiwan. *Taiwan Journal of Forest Science* **25**: 63–80.

Sukumar R, Suresh HS, Dattaraja H, John R, Joshi N. **2004**. Mudumalai forest dynamics plot, India. Tropical forest diversity and dynamism: Findings from a large-scale plot network.551–563.

Šamonil P, Doleželová P, Vašíčková I, Adam D, Valtera M, Král K, Janík D, Šebková B. **2013**. Individual-based approach to the detection of disturbance history through spatial scales in a natural beech-dominated forest (P Cherubini, Ed.). *Journal of Vegetation Science* **24**: 1167–1184.

Vincent JB, Henning B, Saulei S, Sosanika G, Weiblen GD. **2015**. Forest carbon in lowland Papua New Guinea: Local variation and the importance of small trees. *Austral Ecology* **40**: 151–159.

Wang X, Wiegand T, Wolf A, Howe R, Davies SJ, Hao Z. **2011**. Spatial patterns of tree species richness in two temperate forests. *Journal of Ecology* **99**: 1382–1393.

Whittaker RH. **1975**. *Communities and Ecosystems*. New York: MacMillan Publishing Co.

Yuan Z, Wang S, Gazol A, Mellard J, Lin F, Ye J, Hao Z, Wang X, Loreau M. **2016**. Multiple metrics of diversity have different effects on temperate forest functioning over succession. *Oecologia* **182**: 1175–1185.

Zimmerman JK, Comita LS, Thompson J, Uriarte M, Brokaw N. **2010**. Patch dynamics and community metastability of a subtropical forest: Compound effects of natural disturbance and human land use. *Landscape Ecology* **25**: 1099–1111.

Zuleta D, Duque A, Cardenas D, Muller-Landau HC, Davies S. **2017**. Drought-induced mortality patterns and rapid biomass recovery in a terra firme forest in the Colombian Amazon. *Ecology* **98**: 2538–2546.

Zuleta D, Russo SE, Barona A, Barreto-Silva JS, Cardenas D, Castaño N, Davies SJ, Detto M, Sua S, Turner BL ***et al.*** **2020**. Importance of topography for tree species habitat distributions in a terra firme forest in the Colombian Amazon. *Plant and Soil* **450**: 133–149.